Layer Oriented Multi-Conjugate Adaptive Optics systems: Performance analysis by numerical simulations

C. Verinaud[a], C. Arcidiacono[c], M. Carbillet[a], E. Diolaiti[b], R. Ragazzoni[a] , E. Vernet[a], S. Esposito[a]

[a]INAF-Osservatorio Astrofisico di Arcetri, largo E. Fermi 5, I-50125 Florence, Italy.
[b]Dipartimento di astronomia, Vicolo dell'Osservatorio, 2, I-35122 Padova, Italy.
[c]Dipartimento di Astronomia e Scienza dello Spazio, Universita` di Firenze, - Largo E.Fermi 5, I-50125 Firenze, Italy.

ABSTRACT

The multi-conjugate adaptive optics (MCAO) technique allows to correcting the vertical distribution of atmospheric turbulence, extending the isoplanatic angle and the sky coverage. In the Layer-Oriented (LO) approach, each wavefront sensor (WFS) is conjugated to a given atmospheric layer and is linked in closed loop to a deformable mirror, conjugated to the same height. This technique benefits from the co-adding of light coming from the guide stars which can be arbitrarily numerous and faint. In the Multiple Field Of View (MFoV) scheme, each LO WFS is looking through a different field-of-view (FoV) in order to extend even further the sky coverage by increasing the photon density in the various layers. With the help of the CAOS Software Package, upgraded with numerical tools dedicated to MCAO and LO, we simulate the whole wavefront sensing process of a LO system based on pyramid sensors. We describe the modelization of the phenomena occurring during the sensing, such as diffraction effects, and detector noise. Furthermore we also use an independent ad hoc code in order to analyze the performance of the MFoV scheme. The performances are given considering realistic NGS configurations.

Keywords: Multi-Conjugate Adaptive Optics, Layer Oriented, Pyramid wavefront sensor, Multiple Field-of-View, numerical simulations.

1. INTRODUCTION

Multi-Conjugate Adaptive Optics [1] is based on the three-dimensional correction of the turbulence by the means of several deformable mirrors (DM) conjugated to different heights. The Layer Oriented [2] (LO) wavefront sensing approach aims at optimizing the photon density on the wavefront sensors (WFS) detectors by optically co-adding the light coming from different stars. The detectors are located in planes conjugated to the same altitudes as the DMs and each couple WFS-DM is working in an independent closed loop. Recently this technique has been extended to the concept of Multiple Field-of-View (MFoV) [4,5] which consists in the selection of different Field-of-View (FoV) for each WFS, in order to extend the sky coverage. In this paper we give an overview of the simulation packages that are developed to investigate various aspects of the LO wavefront sensing approach: The "Code for Adaptive Optics Systems" (CAOS) [3] software packages has been upgraded to include MCAO and LO, with the aim of building an end-to-end simulation package permitting to simulate the whole measurement process including the diffraction effects of the pyramid wavefront sensor. This package is mainly dedicated to system analysis, and is already used for the development of the first light AO system of LBT [6]. After a description of the model of the pyramid-based LO wavefront sensing, we present a case study for the Multi-conjugate Adaptive Optics Demonstrator (MAD) [7,16]. In particular we validate an interesting feature concerning the calibration of a LO system.
In the third part of this paper we present an independent numerical IDL code that has been developed for the study of the MFoV scheme. This code, based on a simplified model for the wavefront sensing, is faster and permits a more general analysis of the techniques. This simulation code was developed in order to reproduce the main characteristics of a MCAO LO module like MAD. It was first described by Ragazzoni, Farinato & Marchetti (2000) [2] and after by Tordi, Ragazzoni & Diolaiti [8]. It can reproduce the behavior of a classic AO as well as a MCAO system in a LO way, and it is a very useful tool to predict the performances of the adaptive system under some user defined conditions and it allows to determine the free parameters that optimize the system. It follows a simple geometrical approach to simulate wavefront sensing devices. This makes it easy to develop and to upgrade with new characteristics such as the MFoV concept. After an explanation of this

For further information, send correspondence to C. Verinaud (verinaud@arcetri.astro.it)

technique and the description of the situation where this new approach is more useful than single FoV MCAO we analyze the more interesting cases by using the numerical computation.

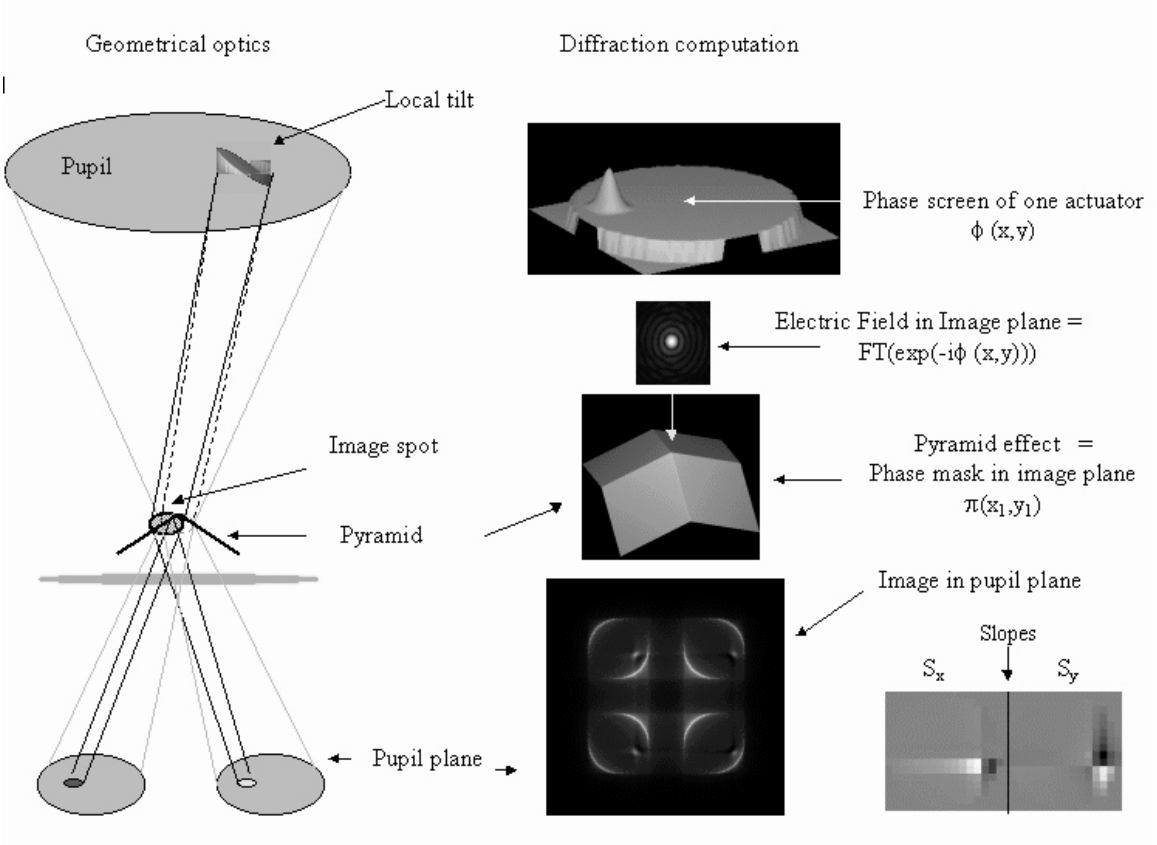

Figure 1. : Simulation of the pyramid sensor. Left : concept in geometrical optics (for a prism). Right : model based on Fraunhofer diffraction theory used in the simulations.

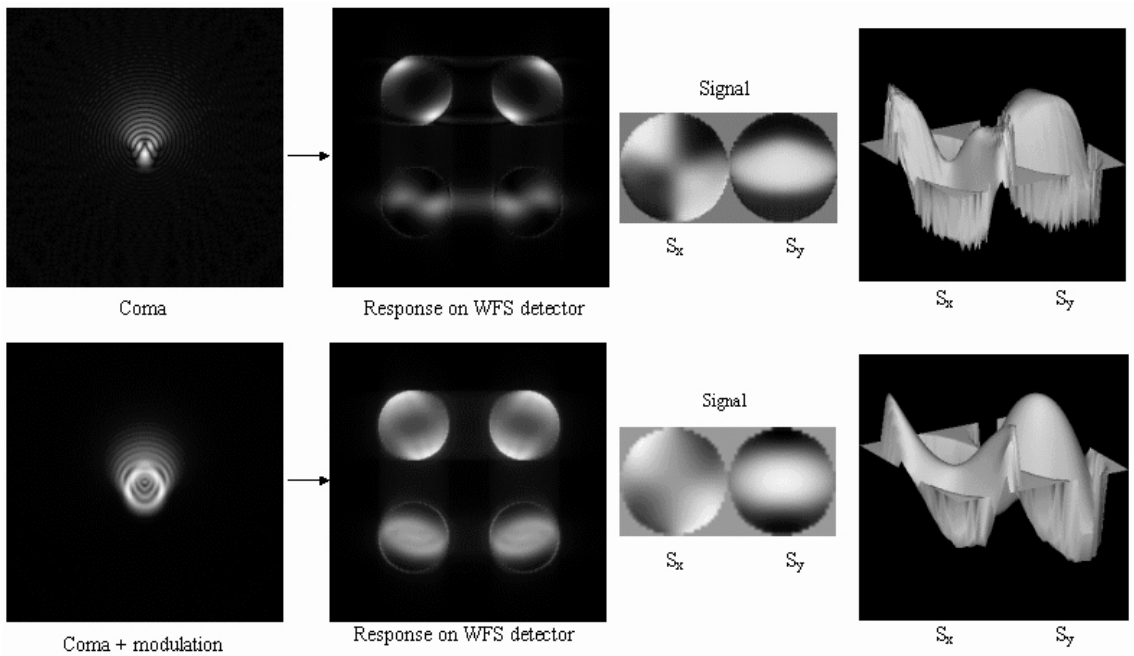

Figure 2: Response of the pyramid sensor to a coma aberration:
Top: without modulation: in this case the strong coma saturates the signal.
Bottom: the image position is modulated on a circle with respect to the pyramid summit: the signal integrated during one modulation cycle is no more saturated, and it is linearized .

2. END-TO-END MODEL FOR PYRAMID LAYER-ORIENTED WAVEFRONT SENSING

End-to-End simulation is a very useful tool for the conception of a complex AO system involving a large number of parameters. Since such a system depends on many physical processes, taking them into account permits to validate with more confidence the choices made during the dimensioning of a project. Moreover it permits to get some useful indications on how the system has to be controlled and optimized either during calibration or for on-sky operation. This is exactly the goal of the CAOS software which packages are being upgraded to multi-conjugate in particular with a pyramid sensor module with layer oriented approach. As it will be emphasized in the next section, the pyramid sensor exhibits important diffraction effects, which may have a non-negligible impact on the performances especially for a diffraction limited regime. We mention here that these effects could even be used for new applications such as for example, wavefront sensing and differential piston measurement for a stellar interferometer with only one pyramid sensor [9], or for the co-phasing of a segmented mirror [10].

2.1 Simulation of the Pyramid Wavefront Sensor

The pyramid sensor invented in 1996 [11] is based on the Foucault test method for optical systems. The main difference with respect to the original Foucault test is the replacement of the knife edge by a glass pyramid whose function is to emulate two knife-edges in two perpendicular directions placed in the focal plane, without wasting light. Figure 1 describes the sensor both in geometrical optics and in Fraunhofer diffraction theory, the latter being used in our simulations. It can be easily shown geometrically, how a local tilt in the incoming wavefront is seen by the wavefront sensor: the left-handed image in Fig.1 shows the travel of the rays coming from a small part of the pupil where the wavefront experiences a local tilt. These rays converge to a spot in the image plane, where is located the summit of the pyramid, represented here for simplicity by a roof prism (only one edge). Because of the tilt, the spot is displaced and covers a larger area on one side of the edge than the other so that more light is deviated in one direction. A difference of illumination is thus occurring in the two pupil images obtained after pupil re-imaging. The difference of intensity in the corresponding regions is directly proportional to the local tilt. In the right part of Fig.1 is described the way the pyramid is simulated: The incoming wavefront $\phi(x,y)$ is here symbolized by a local bump, for example the deformation induced by the actuator of a deformable mirror in a pupil plane. Then, the electric field in the image plane is computed by Fourier transforming the complex amplitude corresponding to the field in the pupil. The pyramid acts on the field in the image plane as a phase mask represented by the function $\Pi(x_1,y_1)$. The final intensity map $I_{pup}(x,y)$ in the pupil plane is obtained by taking the square modulus of the inverse Fourier transform of the image plane complex amplitude taking into account the phase delay induced by the pyramid (Eq.1).

$$I_{PUP} = \left| FFT^{-1} FFT \left[(\exp(-i\phi(x,y)) \times \exp(-i\Pi(x,y))) \right] \right|^2 \quad (1)$$

It has to be noticed that this way to simulate the pyramid WFS is somewhat different from the one done in previous papers [12,13] in which each facet of the pyramid was considered independently as a simple transmission mask. The advantage of this new algorithm, apart that it is faster, is that it permits to take into account the real deviation angles of the pyramid and thus the interferences between the 4 quadrants that depend on their separation. For example, on Fig 1, we can notice that the rims are more brilliant near the center of the whole image in pupil plane because of constructive interferences between the 4 quadrants.

The response of the sensor to the perturbation is a difference in illumination among the 4 pupils at the geometrical location of the actuator. The diffraction effects in the image are important: the pupil is a bit smeared out with brilliant rings, and diffracted light spreads in straight lines from the actuator positions in each pupil. The slope signals S_x and S_y in two perpendicular directions can be defined by Eq 2 :

$$S_x(x,y) = \frac{I_{left}(x,y) - I_{right}(x,y)}{I_{left}(x,y) + I_{right}(x,y)}, \quad S_y(x,y) = \frac{I_{bottom}(x,y) - I_{top}(x,y)}{I_{bottom}(x,y) + I_{top}(x,y)}, \quad (2)$$

where $I_{\text{left(resp. right, top, bottom)}}(x,y)$ is equal to the sum of intensity in the two pupil images in the left (resp. right, top, bottom) part of I_{pup} at point (x,y) in pupil reference for each of the four quadrants. The signal response to one actuator in represented in Fig.1 (right): the diffraction effect is visible as a signal that spreads in the x and y directions from the actuator. Indeed, it can be shown analytically [14] that signal S_x *(resp.* S_y*)* at a given point is given by an integration along *x (resp y)* of $\sin(\phi(x,y))$.

In diffraction limited conditions, the dynamic range for measuring a low order aberration with a pyramid WFS is limited, since the signal reaches very soon a maximum value. This problem is illustrated in Fig.2: When the incoming wavefront is perturbed by a large coma for example, the image on the WFS detector is very contrasted, and the signal is no more proportional to the local derivatives and is almost saturated. To avoid this, it has been shown [11, 15] that it can be convenient to modulate circularly the image position (by introducing a dynamic tilt with the help of a tip-tilt mirror in a pupil plane), in order to redistribute in a smoother way the intensity among

the quadrants and to get into a geometrical and linear regime with a larger dynamical range. The pyramid package of CAOS permits to simulate this modulation with various precisions (number of points in one cycle), depending on the computation time one can allow since I_{pup} has to be computed with Eq.1 and summed up for each position on the modulation cycle.

2.2 Extension to the Layer-Oriented approach

The principles of the Layer Oriented approach for tomographic wavefront sensing is recalled in Fig. 3 (left-handed side): Pyramids are placed at the position of the chosen guide stars which can be arbitrarily numerous as long as there is no mechanical issue. An homothetic copy of the vertical turbulence, is obtained through a simple optical system (pupil re-imager) and a detector is placed at each height conjugated to a deformable mirror. On the right-handed part is explained how this technique is simulated: Let us suppose that 3 guide stars (thus 3 pyramids) are used in the field and that there are two DMs, one in the pupil and one conjugated to for example 10 km. Fig. 3 shows the response on the two WFSs when one actuator is driven in the high conjugated DM and in pupil plane DM. Next to the influence function, is displayed the computed intensity in pupil plane after propagation through each pyramid (obtained with Eq. 1) corresponding to each star. When the high layer DM is driven, the three pyramids see the actuator's influence function at different locations depending on the position of the footprint of each star on this DM, whereas when the DM in the pupil is driven all the pyramids see the same response. To simulate the image on the WFSs we simply apply the geometrical rule of shifting the image of the 4 quadrants for a given star by a vector $\boldsymbol{\theta}.h$ where $\boldsymbol{\theta}$ is the vector-position of the star in the sky with respect to the center of the field and h is the conjugated height of the WFS. The final image on the CCD is the sum of the shifted images of the 4 quadrants for each star. As we can see on Fig. 3, when the high altitude DM is driven, the responses in the high layer sensor is reinforced and 3 attenuated replica are seen in the Ground WFS. We can verify that the corresponding signal is smoothed and thus it can be considered as an additional noise to the measurement, when an aberration is out of focus for a given WFS. The same effect is visible when an actuator is driven in the ground layer: The high layer WFS sees an attenuated and replicated version of the influence function in the pupil DM. We can thus verify that a given WFS sees well an aberration occurring at a height near the conjugated height of the WFS, and is only marginally perturbed by aberrations in far layers.

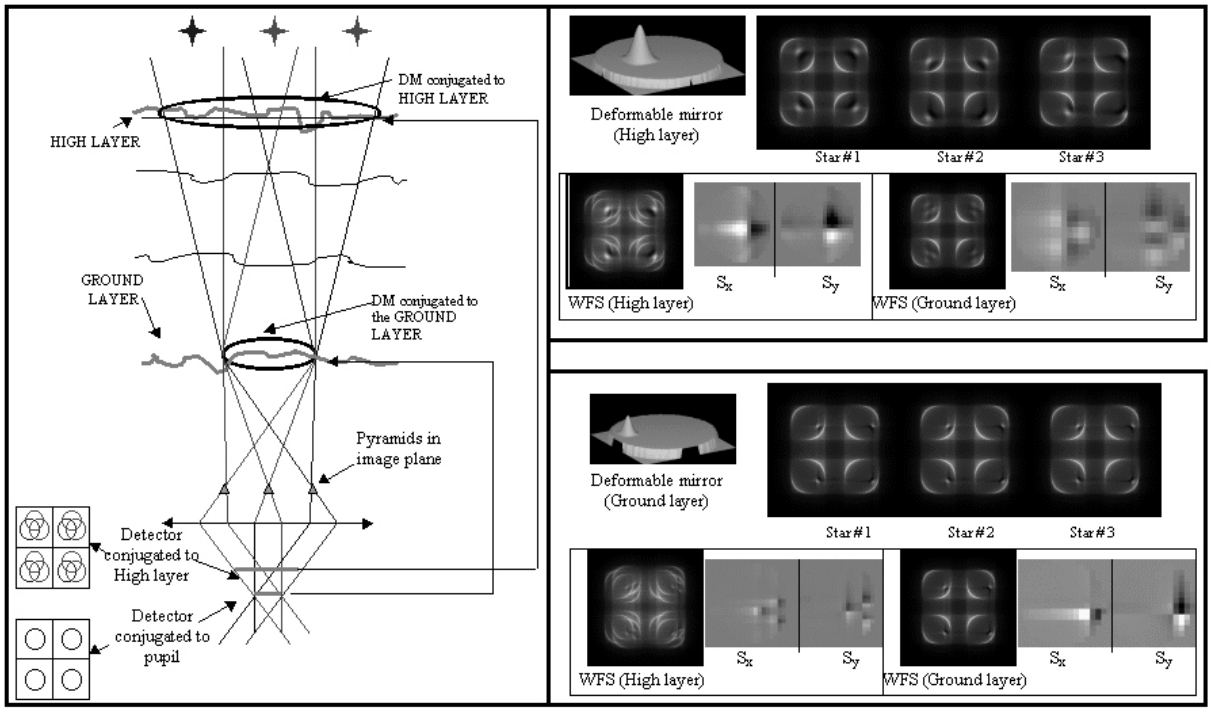

Figure 3. LO concept (Left). Examples of simulated response in respectively the WFS conjugated to the high layer and in the WFS conjugated to the pupil when one actuator is driven in the deformable mirror conjugated to high layer (Top right) and in ground layer (Bottom right)

Once the images on the WFSs are computed, the user can add the usual treatment for computing the final signal: integration on sub-pupil area, addition of sky background, photonisation and addition of detector read-out noise and dark current. In the CAOS package all these parameters can be adjusted with the help of a very user friendly interface. We presented here the optical LO approach, but CAOS permits also to implement the numerical approach (with pyramids or Shack-Hartmann sensors), which differs by the order of the different operations: in the numerical LO approach the noise is added first and the shift of integer number of sub-pupils is applied afterwards.

2.3 A case study : The Multi-conjugate Adaptive optics Demonstrator (MAD)

As an example we give here the results of a simulation for the MAD [7] system of ESO in its LO version [16]. In particular we show how it is possible to calibrate in a very simple way a LO system. Below in table 1 are given the general parameters for the MAD system that have been used in the simulation.

HIGH LAYER	Sensing wavelength: R band (700 nm)
Deformable mirror	60 elements bimorph mirror (@9.2 km)
WFS	Sampling : 9x9 for 2' (binning 4x4)
Read-out noise	3 electrons per frame
Dark current	250 electrons per second
Integration time	2 ms
GROUND LAYER	Sensing wavelength: R band (700 nm)
Deformable mirror	60 elements bimorph mirror (@ 0 km)
WFS	Sampling : 8x8 (binning 2x2)
Read-out noise	4 electrons per frame
Dark current	250 electrons per second
Integration time	2 ms
Overall transmission	0.16

Table 1.

2.3.1 Calibration of a layer-oriented system

An adaptive optics system needs to be calibrated before closing the loop. A very efficient method consists in directly measuring the response of the WFSs to each degree of freedom of the DMs, in order to build an interaction matrix Z whose columns represent the signals (S_x and S_y for slope sensors) for each actuator driven individually. A command matrix C is obtained by a generalized inversion of the interaction matrix:
$C = (Z^T Z)^{(-1)} Z^T$. In a classical MCAO system (one WFS per guide star), the command matrix commands globally the different DMs, from all the measurements for each guide star independently.

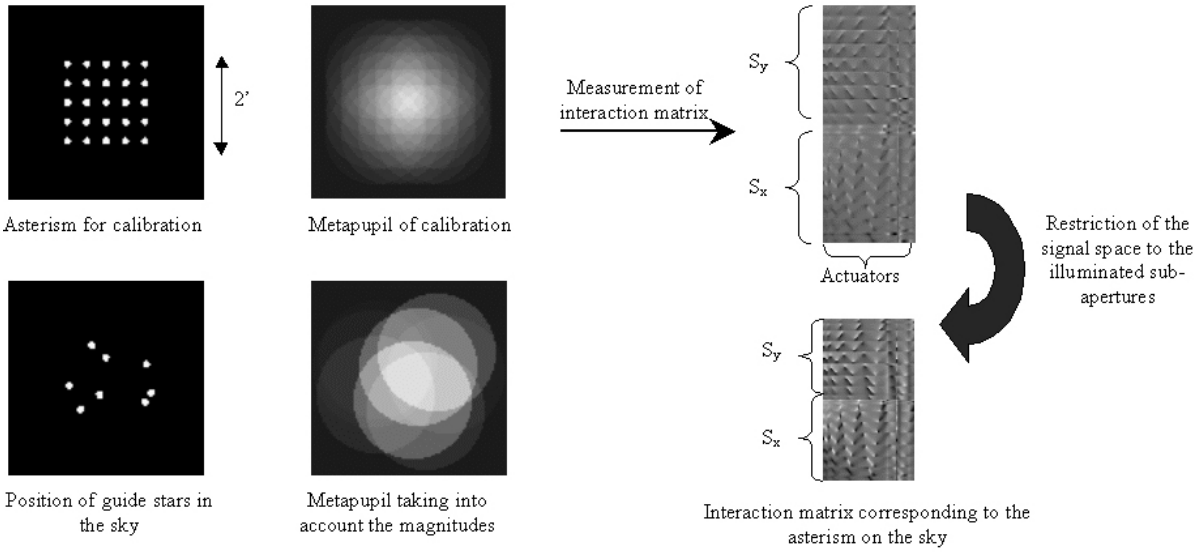

Figure 4. Procedure for the measurement of the calibration matrix and deduction of the interaction matrix corresponding to a given asterism.

For this reason, the interaction matrix will depend on the positions of the guide stars that have a direct influence on the measurements. For a laser guide star system, only a fixed or a few configurations of stars have to be considered. This may be an issue for a system based on natural guide stars for which the positions are random. For MAD in the classical MCAO approach, it is assumed that the system has to be calibrated during day time for each asterism configuration that will be used in closed loop on the sky. We can also imagine to measure the interaction matrices for each WFS for a large number of guide star positions and deduce the real matrix to be used by interpolations, but the precision of this method has still to be studied.
In the layer-oriented approach, the situation is completely different. The procedure used in the simulation is described in Fig. 4. We consider here only the high layer, since the ground layer interaction matrix is equivalent to a classical system. The system has to be calibrated during daytime only once for an asterism (array of artificial stars, fibers), that must illuminate the whole high altitude DM. In our example, an array of 25 stars on an equivalent 2 ' field has been chosen. The corresponding meta-pupil that covers the DM is shown in Fig.4. In this configuration almost the whole CCD of the WFS is covered and an interaction matrix is built with a modulation, in our example, of ± 3λ/D for all pyramids; the calibration measurements are defined on the maximum number of sub-apertures that can be defined in the high conjugated WFS. For any asterism that fits in the 2' field the corresponding interaction matrix that should be used is simply deduced from the calibration interaction matrix by restricting the measurement space of the matrix to the illuminated sub-apertures. No interpolation is needed. The Fig. 4 (bottom) shows the position of the stars, the meta-pupil and the interaction matrix between the sensor and the bimorph influence functions that has been used for the closed loop simulation presented in Fig. 5.

2.3.2 Performance in Closed-Loop

To study the validity of the calibration procedure defined in the precedent section we ran a simple simulation for an 8 stars asterism with magnitudes ranging from 11.5 to 14. The turbulence profile (6 layers) is similar to one measured by Sarazin [17] and for a quite optimistic Fried parameter r_0 (500 nm) = 0.18 m. The chosen wind speeds define an evolution time of 2 ms for the turbulence. As mentioned before, the calibration interaction matrix has been measured with a modulation of ± 3λ/D. However during the correction, no modulation has been used, the image spot size at the sensing wavelength playing itself the role of a certain modulation. It is not obvious that this is optimal but at the status of our knowledge it is the simplest way of operation. The need of modulation during the correction is still an open question that has been addressed in one paper of these proceedings [18]. The results presented in Fig. 5 show that the calibration done in the way presented in this paper permits to close the loop in an efficient way. Further studies will permit to define the eventual limits of this calibration method for example when the residuals are very low at the sensing wavelength (high order systems). In this case, the diffraction effects may play a more important role and the optimal calibration interaction matrix should be measured with a low or even 0 modulation. More over the interaction matrix could be no longer independent of the guide stars asterisms. The role of modulation in closed loop remains also to be better defined.

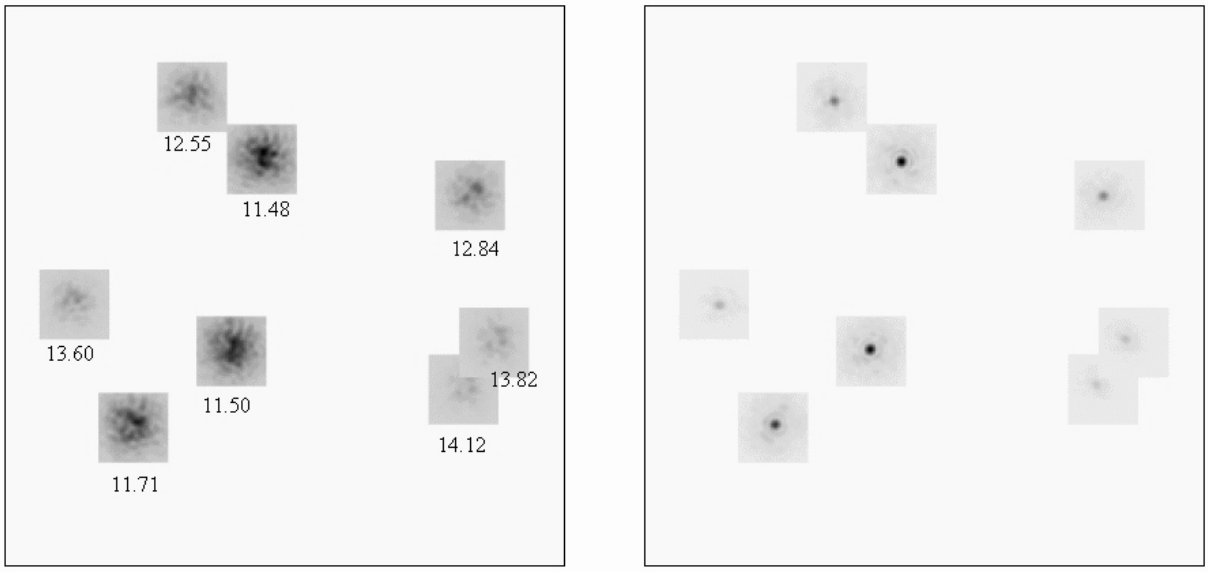

Figure 5. Closed loop results, WFS works at 0 modulation. The FOV is 2'.
Left: guide 8 guide stars with their V magnitudes (without correction)
Right: the same field after correction, long exposure 1 sec. of integration time
The mean Strehl ratio in the Field is 38 % with a peak strehl of 50 % for the brighter stars.

3 INVESTIGATION OF THE MFOV LAYER ORIENTED SCHEME

3.1 The MFoV layer oriented concept

Not all the regions of the sky present a photon density high enough to allow wavefront sensing with the limit imposed by the current astronomical technology. The layer oriented concept goes towards the resolution of this problem: it is able to use the light coming from faint and bright stars by optical co-adding of the light at the conjugation altitude. Anyway, some regions of the sky are not accessible with this approach because of their low stars density.
We said that LO uses the co adding of the light at the different wavefront sensors conjugation altitudes (or DMs heights). In this way each WFS is focused to a particular turbulent layer and it sees only a smoothed version of the layers located at a different height. This smoothing increases with the distance of the layer from the conjugation plane. Placing a DM conjugated to the same plane of the physical aperture of the telescope, the light column of all the guide stars in the FoV overlap perfectly over the telescope pupil, in other words all the NGS are enlightening the same portion of the ground layer and their footprint covers exactly the pupil, while on the high latitude conjugation plane the footprint are displaced of an amount depending on the altitude of the layer and the direction of the GS.
The characteristic of the ground layer to be uniformly enlighten by all the GS in the same way can be exploited to increase the sky coverage by using a different FoV for each conjugation altitude. Every MCAO system, global reconstruction or LO, works to correct the turbulence experienced by the stars inside an angular dimension defined by the corrected FoV. In the MFoV concept the light coming from the stars in a larger FoV, and outside the corrected FoV, can be used to illuminate the ground layer while the light from inner stars is used to enlighten the high conjugation plane [4,5]. In this way the stars located in an annular region with external diameter bigger than the corrected field are the stars illuminating the ground layer WFS, increasing the overall number of photons collected by the wavefront sensor. This system allows to reach higher limiting magnitude, referring only to the magnitude of the stars inside the corrected FoV.
However this larger amount of photons might be paid in terms of achievable correction. Indeed looking towards the stars outside the corrected FoV introduces at the level of the ground DM a smoothed version of the upper layers turbulence that stands outside the corrected FoV. The amount of this external turbulence increases with the heights of the layers, but at the same time this turbulence is more smoothed giving a little overall effect in term of residual phase variance on the detector.
This effect could be corrected by using a third WFS (in a configuration with two DMs) [4] : The first WFS looks to the stars in the annular FoV and drives the DM conjugated to the ground; the second one looks to the stars in the corrected FoV and drives the highest DM. It receives only a fraction of the overall amount of light collected by the telescope: the remaining part will be sent to the third WFS that will be conjugated also to the ground. Its phase measurements will allow the correction of the ground phase residuals coming from the high altitude layer crossed by the light of star in the annular FoV. Such a system can be thought as made by three independent loops, one for the ground layers, one for the high altitude layers and the last for the ground residual of the uncorrected high altitude layers.

3.2 Advantages of MFoV approach

The MFoV idea comes from the attempt to increase the sky coverage for the MCAO applications, and so this approach is particularly useful in the case where it is not possible to find reference stars in the scientific field and when the photon density inside this FoV is too low to supply a good enough signal to noise ratio for the wavefront sensing. When the photon density inside the FoV is high the best correction is achievable using only the stars inside the FoV in order to not introduce the residual phase coming from the high altitude layers. The borderline that delimits the convenience of an option with respect to the other one depends on many parameters such as the atmospheric and system properties. For example very low turbulences allow using long exposure times of the WFS to sense the incoming wavefronts and so it is possible to use very faint stars, with low photon flux, as NGS and the probability to find good reference stars inside the scientific field of view increases. Yet if the wavefront sensor has very bad performances, in terms of read out and dark current, the probability to find NGS decreases and the option to use NGS outside the FoV could be very interesting.

3.3 Simulation code

The simulation code is able to reproduce the main characteristics of a MCAO LO module like MAD. This code was first described by Ragazzoni, Farinato & Marchetti (2000) [2] and after by Tordi, Ragazzoni & Diolaiti

(2001)[8] . It can reproduce the behavior of a classic AO as well as a MCAO system in a layer oriented way, and its development was driven by the objective to obtain a very useful device to predict the performances of an adaptive system under some user defined conditions and it allows to determine the free parameters that optimize this one. The work on this simulation code was performed inside the MAD project. The code was recently implemented to take into account the MFoV approach in the simple case where the number of wavefront sensors is equal to the number of DMs, with no correction of the residuals on the ground DM (see subsection 3.1).
The code is based on the geometrical approximation assumption for the projection of the GSs footprints on the phase screens and on the DM. We simulate the evolution of the phase screens for every temporal interval Δt by shifting the array for the integer part of the movement and by an interpolation for not integer differences. The control algorithm is a pure integrator and for every temporal step the code computes the measured wavefronts of the NGS and then uses them in LO mode to reconstruct the atmospheric layers at the conjugation altitudes of the DMs (and WFSs). The user defines the integration time of the WFSs in terms of number of temporal iterations.
The reconstructed layers are used to compute the shapes of the DMs and, after the temporal steps equivalent to the time necessary to the real system to apply the correction, these ones are subtracted to the wavefronts of the guide stars. One of the advantages to have independent loops with the LO approach is to set the best spatio-temporal sampling referred to the properties of each couple conjugated layers-WFS: the code was conceived in order to manage a number of fully independent loops equal to the number of WFS.
The model used for the wavefront sensor is a phase sensor based on the implementation of the noise propagation coefficients of Shack-Hartmann [19]:

- Photon noise $\sigma^2 = \frac{\pi^2}{2}\frac{1}{n_{ph}}\left(\frac{N_T}{N_D}\right)^2$
- Dark and Ron $\sigma^2 = \frac{\pi^2}{3}\frac{\sigma_e{}^2}{n_{ph}{}^2}\left(\frac{N_S{}^2}{N_D}\right)^2$
- Sky background $\sigma^2 = \frac{\pi^2}{3}\frac{n_{bg}}{n_{ph}{}^2}\left(\frac{N_S}{N_D}\right)^2$

Where $\boldsymbol{n_{ph}}$ is the number of photons detected, σ_e is the rms of electrons due to electronics (it includes RON and dark current rms), $\boldsymbol{N_S{}^2}$ is the total number of pixels per sub-aperture, $\boldsymbol{N_T}$ is the image full width at half maximum (FWHM) and $\boldsymbol{N_D}$ the FWHM of the diffraction pattern of a sub-aperture ($\boldsymbol{N_T}$ and $\boldsymbol{N_D}$ are measured in pixel) and $\boldsymbol{n_{bg}}$ are photons received from the sky background.
The MAD's LO WFS is a pyramid-based wavefront sensor and, in order to reproduce it, we implemented the SH coefficients assuming a modulation of the pyramids that always gives a linear response of this device for every degree of correction and modeling the coefficient $\boldsymbol{N_S}$, $\boldsymbol{N_D}$, and $\boldsymbol{N_T}$ in order to be consistent with the specifics of the pyramid WFS.

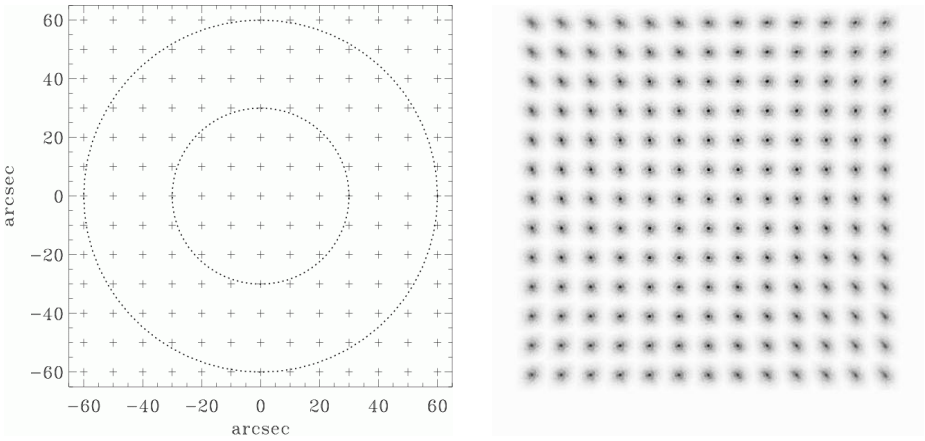

Figure 6. Example of grid of directions where the SR is computed to measure its variation over the field, on the left are presented the long exposure PSF of the stars in the direction of the sky in the figure on the right. The SR is computed as the ratio between the centre value of the array where the Fourier transform of the phase measurements of the stars convolved with the pupil aperture is performed and the value of the same point of the array in the diffraction limited case. In particular this picture refers to the case in Figure 8.

To compute a Strehl Ratio map over the FoV the user defines a grid of "dummy" stars and for each of them the code computes the instantaneous PSF for every temporal step. During the simulation the PSF of a single star is added to the previous one in order to generate a long exposure PSF for every "dummy" star. In this way the code is able to calculate the SR and the PSF for the positions that user set before.

3.4 Simulated cases

Here we present the simulations concerning a study on the MFoV approach opposite to the single FoV LO. We considered as standard for the simulations the system parameters which define the MAD LOWFS[16] module. The MFoV basic structure is characterized by a scientific FoV of 2' where lays an 8 stars real asterism used as driver of the high altitude DM (at 9.2 km from the ground) and an annular FoV with inner and outer radius respectively of 1' and 3'. In this region a 12 stars asterism was posed to drive the ground layer DM. For these simulations we consider only two WFSs, one for each FoV: in this case the starlight coming from every FoV is not split. We always perform a modal reconstruction of the DM shapes from the phase measurements and in the cases under study there were considered all the 59 modes allowable to MAD DMs, (this number is in according to the number of sub-apertures forming the metapupil 60 and 64 for ground and high plane), but excluding the modes which present very low eigenvalues coming from the generalized inversion of the interaction matrix. The integration time for the computation of the long exposure SR was always of 1 second. The other system and atmospheric parameters have been discussed above. All the SR results will refer to the scientific observation band K (@ 2.2 μm).
We considered two different cases of photon density for every case we consider the single FoV and MFoV approaches. In this last case, in order to be conservative, we consider in the annular region a magnitude density lightly bigger (a difference of 0.24 magnitude) than in the central FoV. Between the different simulations the NGS asterism configurations were fixed, we only shifted the magnitude range of the stars adding the same quantities to all the stars, to consider the two different cases of photon density.

R Magnitude density		Stars in the 2' FoV	Magnitude of the stars in the 2'	Stars in the 6' ring	Magnitude of the stars in the 6' ring
2' FoV	6' ring				
15.24	15.47	8	16.52, 18.09, 17.79, 16.81, 15.45, 15.47, 15.68, 17.57	12	14.18, 13.67, 15.61, 15.43, 13.95, 14.57, 14.72, 15.57, 16.07, 16.09, 14.81, 14.85
16.24	16.47	8	17.52, 19.09, 18.79, 17.81, 16.45, 16.47, 16.68, 18.57	12	15.18, 14.67, 16.61, 16.43, 14.95, 15.57, 15.72, 16.57, 17.07, 17.09, 15.81, 15.85

Table 2. Properties of the asterisms used in the simulations performed.

It is important to notice that the in this way the probability to find the described (see Table) amount of light in the central FoV and in the surrounding annular region is almost the same. First, it was necessary to optimize the temporal sampling in the 4 analyzed cases, in order to better confront the two approaches. Some quick simulations were run for a grid of sampling values of 2.5 ms step, and then they were interpolated to obtain the best parameters to be used.

3.5 Results

In the following figures and tables are presented the results. It is easy to see that for the brightest stars case, with an average magnitude of 15.25 in R band by square prime (Figure 7, Figure 8, Table 3) the two techniques are quite equivalent in terms of best performances, both supplying a pick SR of 0.4 while if we keep attention to the uniformity of the SR the MFoV case is preferable being more constant.
In the faintest case (Figure 9, Figure 10, Table 4) the weight of the two approaches is changed: the single FoV suffers from the decreased amount of light from the NGS while MFoV seems to be more robust. It means that MFoV allows a higher limiting magnitude than the single FoV and so a better sky coverage.
In the brightest case the single FoV has a lightly better peak SR that is according to the effect of the residual variance coming from the out of focus projection of the high altitude layer on the ground DM, discussed in the paragraph 3.1.

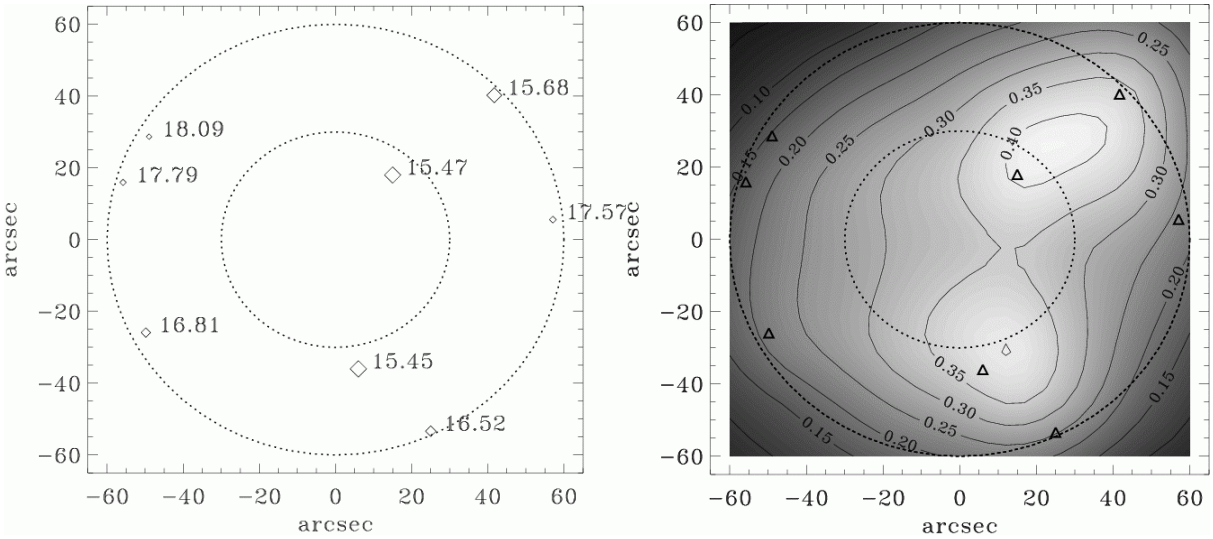

(a) **(b)**

Figure 7. (a) Field map of the natural guide stars of the single FoV case with a single FoV of 2', the two circles have diameters of 1' and 2'. The rumbles define the position of the stars and the numbers on the right are the magnitude in R band. (b) Strehl map of the same case, the NGS directions are indicated by the triangles.

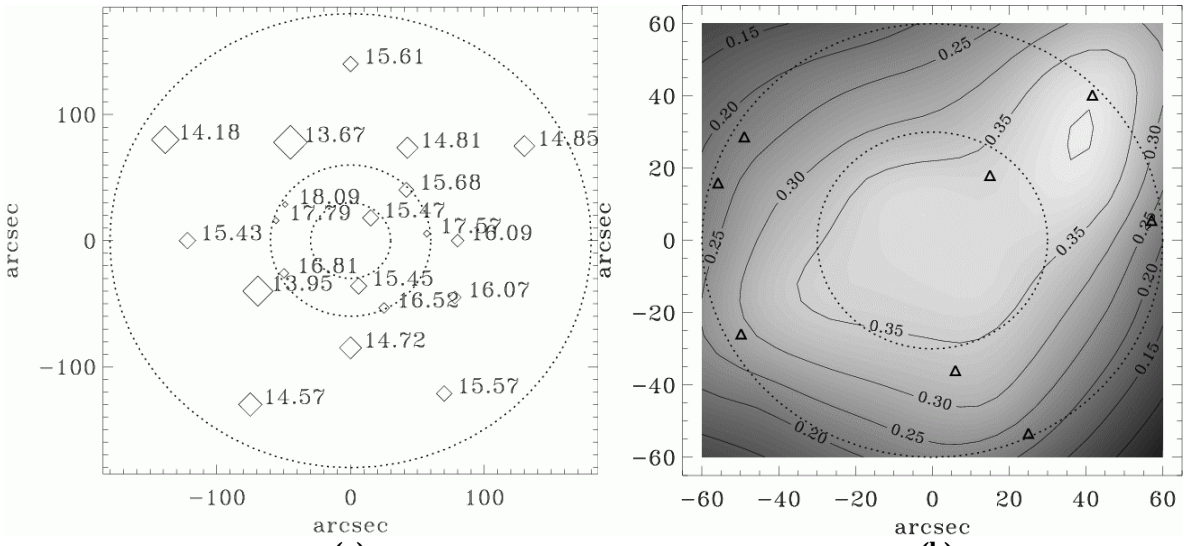

(a) **(b)**

Figure 8. (a) Field map of the natural guide stars of the MFoV case with a inner 2' FoV and 6' FoV of the annular region, the two circles have diameters of 1' and 2'. The rumbles define the position of the stars and the numbers on the right are the magnitude in R band. (b) Strehl map of the same case, the NGS directions are indicated by the triangles.

Case	M_R density [mag_R]/[']	M_R Int NGS	M_R Int on GL-WFS	M_R Int on HL-WFS	Δt integration on WF sensors	Gains	SR on axis long exp.	Max SR Long exp.	Max Instant. SR	Δ SR over FoV [%]
Sing. FoV	15.24	14.00	14.75	14.75	10 ms, 10 ms	0.6, 0.6	0.33	0.42	0.63	74.1 %
MfoV	15.47	11.84	12.00	14.00	5 ms, 10 ms	0.6, 0.6	0.37	0.40	0.63	50.3 %

Table 3. Summary of the cases single FoV and MFoV with a photon density equivalent in R band to a star of 15.24 magnitude by square prime. The second column shows the total integrated magnitude of all the NGS used to drive the adaptive system. The next two columns take in to account the split of the light between wavefront sensors: 50 % to 50 % of the collected light in the single FoV case and inner and outer

FoV stars in MFoV one. In the following: the integration times, the gains used to apply the correction; the values of the SR: at the centre of the FoV and the peak in the long exposure; the peak instantaneous SR; the variation of the SR over the FoV in percentage.

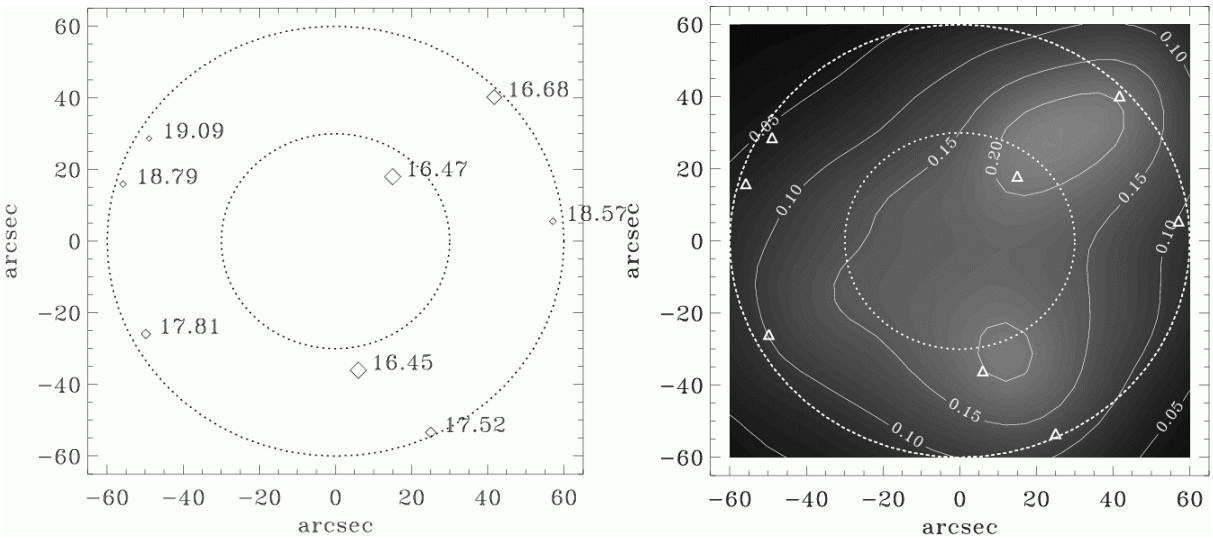

(a) **(b)**

Figure 9. (a) Field map of the natural guide stars of the single FoV case with a single FoV of 2', the two circles have diameters of 1' and 2'. The rumbles define the position of the stars and the numbers on the right are the magnitude in R band. (b) Strehl map of the same case, the NGS directions are indicated by the triangles.

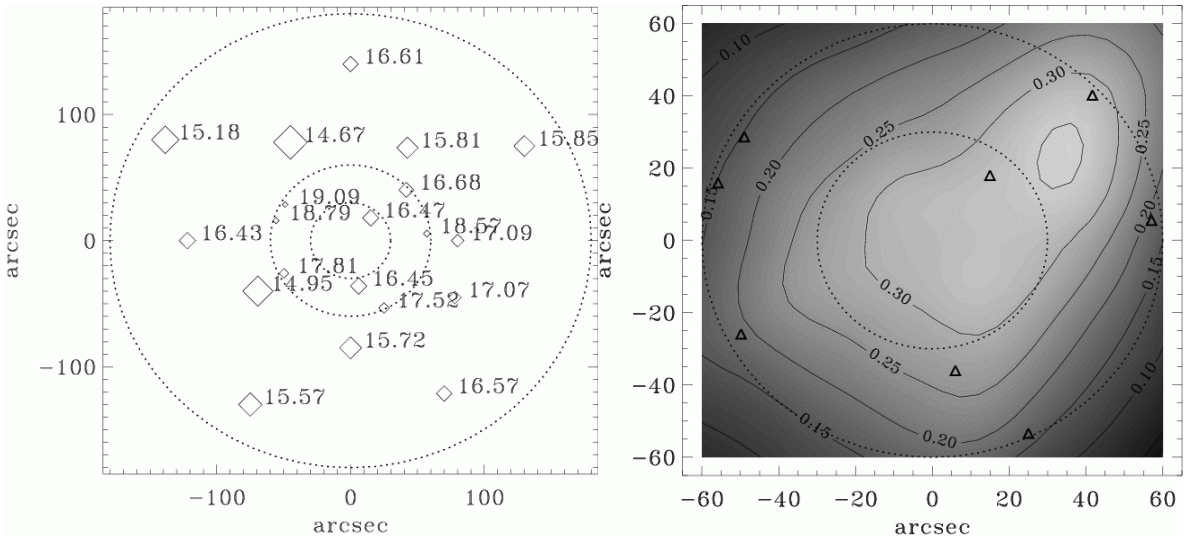

(a) **(b)**

Figure 10. (a) Field map of the natural guide stars of the MFoV case with a inner 2' FoV and 6' FoV of the annular region, the two circles have diameters of 1' and 2'. The rumbles define the position of the stars and the numbers on the right are the magnitude in R band. (b) Strehl map of the same case, the NGS directions are indicated by the triangles.

Case	M_R density [mag_R]/[']	M_R Int NGS	M_R Int on GL-WFS	M_R Int on HL-WFS	Δt integration on WF sensors	Gains	SR on axis long exp.	Max SR Long exp.	Max Instant. SR	Δ SR over FoV [%]
Sing. FoV	16.24	15.00	15.75	15.75	15 ms, 15 ms	0.6, 0.6	0.23	0.17	0.42	83.3 %
MfoV	16.47	12.84	13.00	15.00	6 ms, 12 ms	0.6, 0.6	0.32	0.36	0.63	57.3 %

Table 4. Summary of the results of the cases single FoV and MFoV with a photon density equivalent in R band to a star of 16.24 magnitude by square prime. The second column shows the total integrated

magnitude of all the NGS used to drive the adaptive system. The next two columns take in to account the split of the light between wavefront sensors: 50 % to 50 % of the collected light in the single FoV case and inner and outer FoV stars in MFoV one. In the following: the integration times, the gains used to apply the correction; the values of the SR: at the centre of the FoV and the peak in the long exposure; the peak instantaneous SR; the variation of the SR over the FoV in percentage.

4. CONCLUSIONS

In this paper we have shown the first end-to-end simulation of a pyramid based Layer-Oriented system with the CAOS software, and the first simulations of an MFoV adaptive system with an independent code. We chose for both cases a better than average atmosphere just to analyze simple cases which are not to much demanding for having a realistic sampling of the wavefront (about 2 pixels per r_0 at 700 nm). With the End-to-End model, we are able to simulate the diffraction effects and non-linearity of the pyramid sensor. In particular we have shown that for a LO system the calibration procedure may be much simpler than for classical tomography at least when the correction is not diffraction limited. Further investigations are pursued to precise the role of modulation during the closed loop operation. Indeed it has been suggested by several works that closing the loop is almost always possible without any modulation. However, modulating the pyramids in closed loop could still help in optimizing the correction by balancing the effect of non-linearity and noise propagation .

The study on MFoV shows that this technique is able to increase the sky coverage by using a larger FoV than single FoV in all the poor stars density cases. We show that the two approach are quite equivalent when there are enough bright stars in the corrected FoV while the MFoV approach allows to achieve better result when the star density is lower. In any case MFoV technique permits to obtain a more uniform corrections in the central FoV.

ACKNOWLEGEMENTS

C.V. is supported by the European Union through the Research and Training Network for “Adaptive Optics for Extremely Large Telescopes “ under contract # HPRN-CT-2000-00147.

REFERENCES

1. Beckers J.M.,”Increasing the size of the isoplanatic patch with Multi-Conjugate adaptive optics”, Proceedings on Very Large Telescopes and their instrumentation, M.-H. Edition, 30, 693, ESO Proceedings, Garghing, 1988.
2. Ragazzoni, Roberto; Farinato, Jacopo; Marchetti, Enrico,2000 ,Proc. SPIE Vol. 4007, p. 1076-1087, Adaptive Optical Systems Technology, Peter L. Wizinowich; Ed.
3. Carbillet M.; Correia S., Femenia B.; Riccardi A., 2000, Proc. SPIE Vol. 4007, p. 155-166, "Adaptive Optical Systems Technology", Peter L. Wizinowich; Ed.
4. Ragazzoni R., Diolaiti E., Farinato J., Fedrigo E., Marchetti E., Tordi M. and Kirkman D., “Multiple Field of View layer oriented”, in *ESO proceedings of the Venice conference on Beyond Conventional Adaptive Optics*, R. Ragazzoni, N. Hubin and S. Esposito, eds., in publication., 2001a
5. Ragazzoni R., Diolaiti E., Farinato J., Fedrigo E., Marchetti E., Tordi M. and Kirkman D., “Multiple Field of View layer oriented adaptive optics”, *A&A submitted*, 2001b.
6. Esposito S., A. Tozzi, D. Ferruzzi, M. Carbillet, A. Riccardi, L. Fini, C. Verinaud, M. Accardo, G. Brusa, D. Gallieni, R. Biasi, C. Baffa, V. Biliotti, I. Foppiani, A. Puglisi, R. Ragazzoni, P. Ranfagni, P. Stefanini, P. Salinari, W. Seifert, J. Storm, “First Light AO system for LBT”, this conference
7. E. Marchetti, N. N. Hubin, E. Fedrigo, R. Donaldson, R. Conan, M. Le Louarn, B. Delabre, F. Franza, D. Baade, C. Cavadore, A. Balestra, J.-L. Lizon, R. Ragazzoni, J. Farinato, E. Vernet-Viard, E. Diolaiti, D. J. Butler, S. Hippler, A. Amorin, “MAD the ESO Multiconjugate Adaptive Optics Demonstrator”, this conference
8. Tordi M., Ragazzoni R. and Diolaiti E., “Simulation of a Layer-Oriented MCAO system ”, in *ESO proceedings of the Venice conference on Beyond Conventional Adaptive Optics*, in publication., 2001c.
9. Verinaud, C.; Esposito, S, Optics Letters, vol. 27, Issue 7, pp.470-472
10. Esposito, S.; Devaney, N., "Beyond Conventional Adaptive Optics", proceeding of the conference held in Venice, on May 7-10, 2001, to be published by European Southern Observatory
11. Ragazzoni R., 1996, J. Mod. Opt. 43, 289
12. Ragazzoni, R. Farinato, J., Astron. Astrophys. 350, L23-L26 (1999)
13. Esposito, S.; Riccardi, A., Astronomy and Astrophysics, v.369, p.L9-L12 (2001)
14. Riccardi,A., Esposito, S., in preparation.
15. Riccardi, A., Bindi, N., Ragazzoni, R., Esposito, S., & Stefanini, P. 1998, Proc. SPIE, 3353, 941
16. E. Vernet-Viard, R. Ragazzoni, E. Diolaiti, R. Falomo; J. Farinato, E. Fedrigo, E. Marchett,C. Arcidiacono, A. Baruffolo; S. Esposito, M. Tordi, M. Carbillet, C. Verinaud, this conference
17. Sarazin M., ``Site atmospheric characterization,", ESO Proc. Topical Meeting on Adaptive Optics, 1996.
18. Costa, J, R. Ragazzoni, S. Hippler, A. Ghedina, J. Farinato, this conference
19. Rousset, G.,”Wave-front sensor” in *Adaptive Optics in Astronomy*,p115-117, Roddier F. editor, 1999.